Effect of cationic substitutions on the photoluminescence properties of Eu2+ doped SrCN2 prepared by a facile C3N4 based synthetic approach

Erwan Leysour de Rohello, Yan Suffren, Odile Merdrignac-Conanec, Olivier Guillou, François Cheviré

Effect of cationic substitutions on the photoluminescence properties of Eu^{2+} doped $SrCN_2$ prepared by a facile C_3N_4 based synthetic approach

Erwan Leysour de Rohello*, Yan Suffren, Odile Merdrignac-Conanec, Olivier Guillou, François Cheviré

Univ Rennes 1, INSA Rennes, CNRS, ISCR (Institut des Sciences chimiques de Rennes) – UMR 6226, F-35000 Rennes, France

Abstract

An alternative general approach to synthesize carbodiimide materials using carbon nitride as precursor is proposed. This new facile synthetic route was illustrated by the preparation of single phases α-$SrCN_2$ and β-$SrCN_2$ in a reproducible and effective manner *via* the substitution of barium and calcium for strontium. Structural characterizations and optical properties of Eu^{2+} doped $SrCN_2$ polymorphs were investigated on the bases of high-resolution X-ray powder diffraction and photoluminescence analyses to evaluate the potential of such systems as red phosphors. All Eu^{2+} doped samples exhibit intense red emission in the 620-630 nm range when excited at 440 nm at 77 K with little impact of the crystal lattice on emission wavelength. However, calcium and barium substitutions for strontium strongly impact the emission intensity and the emission width respectively and all doped samples have their emission intensity reduced by 50 % around 80-90 K and totally quenched at RT.

Keywords: Alkaline-earth, Carbodiimide, Carbon nitride, Luminescence, Phosphor

1. Introduction

Solid-state lighting using light emitting diodes is recognized as a major disruptive technology for the next generation of lighting [1, 2]. Over the past decade, concerted efforts have been in progress for the development of new materials with good performance what can lead to a significant decrease of the manufacturing cost. In this context, alkaline-earth carbodiimides materials received a lot of attention recently for their potential application as hosts for luminescent materials, especially for red phosphors [3, 4, 5, 6]. Several crystal structures have been reported for alkaline-earth (AE) carbodiimides $AECN_2$ (AE = Mg, Ca, Sr and Ba): rhombohedral lattice ($R\bar{3}m$ (n°166): $MgCN_2$, $CaCN_2$ and β-$SrCN_2$; $R\bar{3}c$ (n°167): $BaCN_2$), orthorhombic lattice (*Pnma* (n°62): α-$SrCN_2$) and tetragonal lattice (*I4/mcm* (n°140): $BaCN_2$) [5, 7, 8]. Figure 1 shows the crystal structure of both $SrCN_2$ polymorphs. In α-$SrCN_2$, the Sr^{2+} cation is octahedrally coordinated by nitrogen atoms, however, $[N=C=N]^{2-}$ carbodiimide units in two orientations built up layers parallel to the (010) plane. The octahedra are connected *via* edges and corners sharing and by $[N=C=N]^{2-}$ carbodiimide units. In β-$SrCN_2$, the Sr^{2+} cation is also octahedrally coordinated by nitrogen atoms, however, the edge-sharing octahedra form layers within (001) plane and are connected by $[N=C=N]^{2-}$ carbodiimide units parallel to each other along the c-axis.

In general, Sr-based compounds are ideal host lattices for Eu^{2+} ions due to their comparable ionic radii and identical charge. The emission spectra of Eu^{2+} are usually characterized by electronic transitions from $4f^6 5d^1$ to $4f^7$ states. Since the involved 5d orbitals are external, the position of these energy levels and consequently the wavelengths of excitation and emission bands strongly depend on the host lattices [9]. Recently, luminescent properties of Eu^{2+} doped α-$SrCN_2$ have been reported [3, 4]. However, the stabilization of Eu^{2+} doped β-$SrCN_2$ has not been evidenced yet especially because low temperatures (< 700 °C) are required for the synthesis of β-$SrCN_2$ while high temperatures are preferred for the reduction of Eu^{3+} to Eu^{2+} into the matrix. In this work, first we report a new synthetic route for carbodiimide materials using C_3N_4 as a carbon and nitrogen source, illustrated with the case of $SrCN_2$ phosphors, and we discuss the impact of the structure, *via* Ba^{2+} and Ca^{2+} substitution for Sr^{2+}, on the $^{2+}$ doped $AECN_2$ luminescent properties.

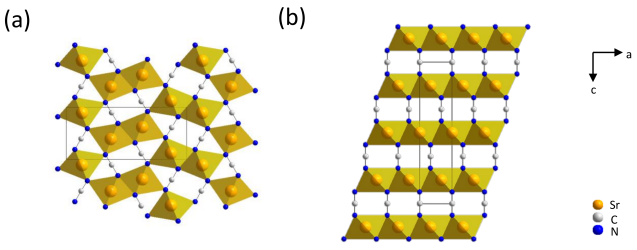

Figure 1: Crystal structures of α-$SrCN_2$ (a) and β-$SrCN_2$ (b) with SrN_6 octahedra given in light orange, Sr atoms in orange, C atoms in gray, and N atoms in blue.

*Corresponding author

Email address: erwan.leysour@univ-rennes1.fr (Erwan Leysour de Rohello)

2. Experimental procedure

2.1. Preparation of alkaline-earth carbodiimides

Powder samples with the general formula $SrCN_2$, $Sr_{0.98}Eu_{0.02}CN_2$, $Sr_{0.93}Ba_{0.05}Eu_{0.02}CN_2$ and $Sr_{0.93}Ca_{0.05}Eu_{0.02}CN_2$ were synthesized through solid-state reaction from (doped) strontium carbonate and carbon nitride (C_3N_4). 4 g of undoped or doped strontium carbonate precursors ($SrCO_3$, $Sr_{0.98}Eu_{0.02}CO_3$, $Sr_{0.93}Ba_{0.05}Eu_{0.02}CO_3$ and $Sr_{0.93}Ca_{0.05}Eu_{0.02}CO_3$) were prepared by co-precipitation method using $SrCl_2{\cdot}6H_2O$ (Acros Organics, $\geqslant$99%), $BaCl_2{\cdot}H_2O$ (Aldrich, $\geqslant$99.9%), $CaCl_2{\cdot}6H_2O$ (Aldrich, 98%), $Eu(NO_3)_3{\cdot}6H_2O$ (Alfa Aesar, 99.9%) and Na_2CO_3 (Acros Organics, 99.95%) as raw materials. Appropriate amounts of alkaline-earth chlorides and europium nitrate were dissolved in 100 mL of deionized water until obtaining a homogeneous solution, which was then added drop-wise into a 100 mL sodium carbonate solution (molar ratio Na/AE = 1.5) under vigorous stirring. A white precipitate was formed and separated from the solution by centrifugation at 4000 rpm for 5 min with intermediate rinsing with deionized water (x3) then ethanol (x2) in order to remove any unprecipitated impurities. Finally, the resulting precipitate was dried in an oven at 80 °C overnight to obtain the (doped) strontium carbonate powder precursor. Carbon nitride (C_3N_4) powder was synthesized by heating melamine in muffle furnace. In a typical synthesis run, 15 g of melamine (Aldrich, 99%) was placed into a capped alumina crucible and then heated up to 550 °C for 5 h with a heating rate of 3 °C min^{-1}. The as obtained yellow product was collected and ground into powder for further use (see figure S1 for XRD patterns of the as prepared carbonates and carbon nitride). All carbodiimide samples have been synthesized according to the following procedure. 500 mg of undoped or doped strontium carbonate was thoroughly mixed with 2 g of carbon nitride in an agate mortar. The resulting mixture was placed in an open alumina crucible and loaded in a tubular furnace under nitrogen flow (N_2). The furnace was purged during 15 min before switching to ammonia (NH_3) with a flow rate of 12 L h^{-1}. Then the mixture was heated at 800 °C for 1 h with a heating rate of 10 °C min^{-1}. Thereafter, the tubular furnace was turned off and allowed to cool down to room temperature. Finally, the product was transferred and stored in a glovebox. Let us note that NH_3 atmosphere was necessary to remove carbon residues during the heat treatment.

2.2. Characterizations

X-ray diffraction (XRD) patterns were recorded at room temperature in the 2θ range 10-90° with a step size of 0.0261° and a scan time per step of 40 s using a PANalytical X'Pert Pro diffractometer (Cu-L2,L3 radiation, λ = 1.5418 Å, 40 kV,40 mA, PIXcel 1D detector). Data collector and HighScore Plus softwares were used, respectively, for recording and analysis of the patterns. The purity of all the prepared powdered materials was systematically checked by XRD. The powder XRD patterns for Rietveld refinements were collected at room temperature in the 2θ range 5-120° with a step size of 0.0131° and a scan time per step of 200 s. All calculations were carried out with Fullprof and WinPlotr programs [10, 11]. The pseudo-Voigt profile function was used and the background was approximated by linear interpolation between a set of background points. The lattice parameters were obtained from Rietveld refinements considering the space group *Pnma* (n°62) for the α-phase and $R\bar{3}m$ (n°166) for the β-phase. Strontium, europium and calcium (or barium) were considered occupying the same crystallographic site with respective site occupancies calculated from the targeted chemical compositions. The same thermal parameter was applied for all atoms occupying the strontium site and the site occupancies were not refined. The estimated standard deviations (ESD) were corrected using the Berar and Lelann coefficient calculated from the structure refinement [12, 13]. Energy dispersive X-ray spectroscopy (EDS) investigations were performed using a JEOL IT300 microscope operating at 10mm working distance with an accelerating voltage of 20 kV and a probe current of 7.45 nA. Sample preparation consisted in depositing the powder on a carbon tape then metallization with gold. Nitrogen and oxygen contents were determined with a LECO TC-600 Analyzer using the inert gas fusion method in which nitrogen and oxygen contents were measured as N_2 by thermal conductivity and as CO_2 by infrared detection respectively. Diffuse reflectance (DR) spectra were collected using a Varian Cary 100 Scan spectrometer equipped with a Varian WinUV software and the integrating sphere Lab-sphere (DRC-CA-30). Experimental data were collected within the 250-800 nm range with a 1 nm step. Band gaps of the materials (Eg) were calculated using the Kubelka-Munk formalism [14]. Solid-state excitation and emission spectra were measured with a Horiba Jobin-Yvon Fluorolog-III fluorometer equipped with a Xe lamp 450 W and a UV-Vis photomultiplier (Hamamatsu R928, sensitivity 190-860 nm). Luminescence at various temperatures (77-197 K) has been measured on powder samples mounted directly onto copper plates using conductive silver glue and cooled with an optical cryostat (Oxford OptistatCF) coupled to a liquid nitrogen bath able to reach temperatures down to 77 K under nitrogen atmosphere.

3. Results and Discussion

3.1. Toward a new simple and efficient synthetic route for carbodiimide materials using C_3N_4

Up to date, alkaline-earth carbodiimides have been prepared thanks to a variety of chemical routes. For instance, $AECN_2$ (AE = Mg, Sr, Ca) can be prepared from melamine ($C_3N_6H_6$) and metal nitrides (Mg_3N_2, Sr_2N, Ba_3N_2) at temperatures between 740 and 850 °C under argon atmosphere [7]. $SrCN_2$, $BaCN_2$ and $CaCN_2$ can also be obtained from the reaction of their corresponding carbonates under an ammonia flow at high temperatures [3, 5, 15]. Additionally, solid-state metathesis reactions have also resulted in the formation of $SrCN_2$ from SrI_2 and $ZnCN_2$ between 570 and 700 °C for 24 h or $CaCN_2$ from and $Li_2(CN_2)$ at 500 °C for 48 h [6, 16]. Finally, metallic flux route have also been applied to prepare $SrCN_2$ by a reaction of strontium iodide, cesium cyanide, and cesium azide at 800 °C for

24 h [4]. In our preliminary investigations, cyanamide (H_2CN_2, Aldrich, 99%) and strontium carbonate ($SrCO_3$, Aldrich, 99.9%) were used as starting materials for the preparation of $SrCN_2$. The XRD patterns of the products obtained from mixtures of H_2CN_2 and $SrCO_3$ (mass ratio H_2CN_2 : $SrCO_3$ = 1 : 2) at various temperatures (200 - 700 °C) for 2 h under NH_3 flow (12 L h^{-1}) are displayed in Figure S2. Upon heating, condensation of cyanamide into dicyanamide, melamine, melem (triamino-tri-s-triazine) occurred prior to the conversion of $SrCO_3$ into $SrCN_2$ at 500 °C. Such thermal evolution of cyanamide is in agreement with previous report in literature about the formation of carbon nitride C_3N_4 [17]. Additionally, a large part of the cyanamide rapidly sublimed out of the samples to condense as melamine at the cold end of the furnace. Therefore, hereafter carbon nitride has been used as a carbon and nitrogen source for the synthesis of carbodiimide materials. The use of carbon nitride which starts to decompose at temperature above 600 °C [17], as precursor instead of cyanamide led to a better efficiency and control of the carbonate to carbodiimide conversion under our experimental conditions. In order to confirm the effectiveness of this new approach, we have performed three synthesis runs at temperatures ranging from 600 to 800 °C for 1 h under NH_3 flow using $SrCO_3$ and C_3N_4 freshly prepared as precursors. The crystal structure and purity of samples were checked by X-ray diffraction (Figure 2. The patterns show that all the products are crystallized. At 600 °C, the sample presents a mixture of α- and β-$SrCN_2$ phases (JCPDS card no. 82-0988 and JCPDS card no. 220-4348, respectively) with trace of undecomposed organic byproducts while at 700 °C sample shows phase-pure α-$SrCN_2$. The sample heated at 800 °C exhibit at first glance phase-pure α-$SrCN_2$, however a closer look at the XRD patterns reveals the presence of two extra peak shoulders at $\sim$ 17.69° and 28.54° in 2θ attributed to β-$SrCN_2$ phase. Such results are in good agreement with the literature which refers to a $\beta \rightarrow \alpha$ phase transition between 620 and 700 °C [16, 18]. Nevertheless, β-$SrCN_2$ remains difficult to stabilize without α-$SrCN_2$ contamination [4, 16].

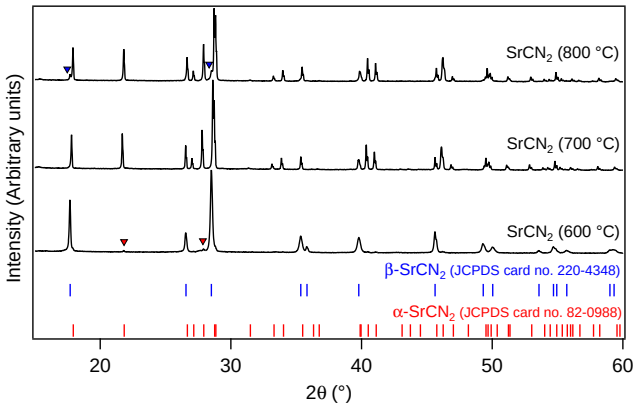

Figure 2: The X-ray diffraction diagrams of $SrCN_2$ samples synthesized at different temperatures (from 600 to 800 °C). Blue triangles indicate extra-peaks corresponding to β-$SrCN_2$ phase while red triangles indicate extra-peaks corresponding to α-$SrCN_2$.

3.2. *Effect of cationic substitutions on Eu^{2+} doped $SrCN_2$ crystal structure*

In order to compare the role of the crystal structure type on the photoluminescence properties of Eu^{2+} doped $SrCN_2$, we attempted to synthesize Eu^{2+} doped α- and β-polymorphs using the same experimental conditions, i.e. at 800 °C for 1 h. To do so, we looked at the impact of cationic mean size as both crystal structure types exhibit a single crystallographic site for the alkaline-earth cation with slightly different volumes. Indeed, based on the crystal structures parameters reported by Krings et al. [4] for both α- and β-$SrCN_2$, calculated volumes for the octahedral cationic site are 23.46 Å^3 and 23.05 Å^3 respectively. We can then expect that substituting Ba^{2+} ($r_{Ba^{2+}}$ = 1.35 Å) and Ca^{2+} ($r_{Ca^{2+}}$ = 1.0 Å) for Sr^{2+} ($r_{Sr^{2+}}$ = 1.18 Å), i.e. increasing or lowering the alkaline-earth mean size, could stabilize the α- or β-type crystal structure respectively. $Sr_{0.98}Eu_{0.02}CN_2$, $Sr_{0.93}Ba_{0.05}Eu_{0.02}CN_2$ and $Sr_{0.93}Ca_{0.05}Eu_{0.02}CN_2$ were prepared under the same conditions. The XRD patterns of the samples are depicted in Figure 3. As anticipated, $Sr_{0.93}Ba_{0.05}Eu_{0.02}CN_2$ presents phase-pure α-$SrCN_2$ while $Sr_{0.93}Ca_{0.05}Eu_{0.02}CN_2$ shows phase-pure β-$SrCN_2$ without any traces of secondary phases. Let us note that the $Sr_{0.98}Eu_{0.02}CN_2$ sample also exhibits the α-type structure. Moreover, elemental analyses showed that nitrogen contents in $SrCN_2$, $Sr_{0.98}Eu_{0.02}CN_2$, $Sr_{0.93}Ba_{0.05}Eu_{0.02}CN_2$ and $Sr_{0.93}Ca_{0.05}Eu_{0.02}CN_2$ were determined to be 22.57, 21.95, 21.32 and 22.11 %wt respectively which are in line with those calculated values: 21.94, 21.72, 21.81 and 22.13 %wt. The oxygen amount in each sample did not exceed 0.3 %wt. EDS analyses confirm that the targeted cationic substitutions have been effective (see Table S1). The powder diffraction data of the as prepared samples were analyzed by Rietveld refinement. Final Rietveld refinement patterns of $Sr_{0.93}Ba_{0.05}Eu_{0.02}CN_2$ and $Sr_{0.93}Ca_{0.05}Eu_{0.02}CN_2$ are presented in figure S3 and S4 while the crystal structure parameters and details of the refinement as well as the atomic parameters are listed in Tables 1 and 2.

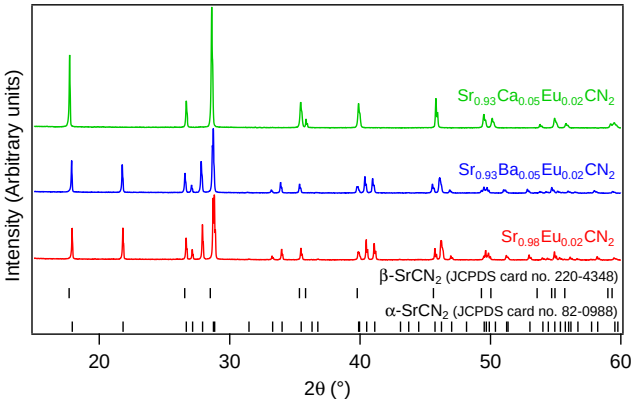

Figure 3: The X-ray diffraction diagrams of Eu^{2+} doped $SrCN_2$ samples ($Sr_{0.98}Eu_{0.02}CN_2$, $Sr_{0.93}Ba_{0.05}Eu_{0.02}CN_2$ and $Sr_{0.93}Ca_{0.05}Eu_{0.02}CN_2$, red, blue and green curves, respectively).

$SrCN_2$ and $Sr_{0.98}Eu_{0.02}CN_2$ exhibit very close lattice parameter values due to comparable cation radii ($r_{Sr^{2+}}$ = 1.18 Å vs. $r_{Eu^{2+}}$ = 1.17 Å). However as displayed in table S2,

Table 1: Details of the Rietveld refinement of of $SrCN_2$, $Sr_{0.98}Eu_{0.02}CN_2$, $Sr_{0.93}Ba_{0.05}Eu_{0.02}CN_2$ and $Sr_{0.93}Ca_{0.05}Eu_{0.02}CN_2$.

Compound	$SrCN_2$	$Sr_{0.98}Eu_{0.02}CN_2$	$Sr_{0.93}Ba_{0.05}Eu_{0.02}CN_2$	$Sr_{0.93}Ca_{0.05}Eu_{0.02}CN_2$
Space group (n°)	Pnma (62)	Pnma (62)	Pnma (62)	$R\bar{3}m$ (166)
Z	4	4	4	3
Lattice parameters				
a (Å)	12.4247(3)	12.4232(3)	12.4454(2)	3.9583(1)
b (Å)	3.9647(1)	3.9641(1)	3.9793(1)	3.9583(1)
c (Å)	5.3949(1)	5.3953(1)	5.4075(1)	15.0202(5)
Volume (Å^3)	265.75(1)	265.70(1)	267.81(1)	203.82(1)
Rp (%)	16.1	15.8	13.4	14.4
Rwp (%)	12.6	12.2	9.96	11.7
Rexp (%)	7.27	7.26	7.72	6.41
χ^2	2.99	2.80	1.66	3.33

strong disparity is observed between the Sr–N bond lengths (maximum/minimum lengths are 2.706/2.575 Å and 2.745/2.583 Å for the undoped and Eu^{2+} doped samples respectively) associated with a noticeable asymmetry of the C–N bonds (i.e. 1.256/1.178 Å and 1.255/1.134 Å, respectively). Those results differ slightly from literature data which report usually a more symmetrical carbodiimide unit for α-$SrCN_2$ [7, 16]. Structural refinement results concerning Ba^{2+} substituted sample show an increase of cell parameter values which confirms the insertion of Ba^{2+} in our doped sample. Moreover, we notice that the Sr–N bond lengths disparity is less important with a much more symmetrical carbodiimide unit. The average Sr–N and C–N bond lengths were determined to be 2.638 Å and 1.234 Å respectively, which are in good agreement with those already found for the α-$SrCN_2$ compound [4, 7, 16]. In the case of Ca^{2+} substituted sample, the slight decrease of refined cell parameters compared to those reported by Liao et al. [8] (a = b = 3.9732(5) Å and c = 15.028(3) Å) confirms the insertion of Ca^{2+} within the structure. Moreover, symmetrical C–N bond length was determined to be 1.232 Å which is similar to the Ba^{2+} substituted $SrCN_2$ compound.

3.3. Diffuse reflection spectra

Figure 4 shows the diffuse reflection spectra of undoped and Eu^{2+} doped $SrCN_2$ samples. Undoped $SrCN_2$ compound shows a drastic drop in reflection in the UV range around 280 nm with an estimated band gap at about 4.56 eV, corresponding to the valence-to-conduction bands transitions of the $SrCN_2$ host lattice in agreement with a previous report [3]. The intense reflection in the visible spectral range is in agreement with the observed white daylight color of undoped $SrCN_2$. For Eu^{2+} doped samples, two broad absorption bands can be observed in the wavelength ranges of 280-320 and 320-500 nm, respectively. Due to the absence of such bands in undoped $SrCN_2$, both of them can be attributed to the 4f-5d absorption of Eu^{2+} ions. As a consequence of the strong absorption of Eu^{2+} bands up to the visible range, the daylight colour of $Sr_{0.98}Eu_{0.02}CN_2$ and $Sr_{0.93}Ba_{0.05}Eu_{0.02}CN_2$ compounds is bright yellow (optical band gap = 2.46 eV) while a deeper yellow colour is observed for $Sr_{0.93}Ca_{0.05}Eu_{0.02}CN_2$ (optical band gap = 2.30 eV). Concomitantly the onset of the reflection drop of the Ca^{2+} substituted sample significantly shifts to a longer wavelength (~550 nm) in comparison to the edge of $Sr_{0.98}Eu_{0.02}CN_2$ and $Sr_{0.93}Ba_{0.05}Eu_{0.02}CN_2$ compounds (~500 nm). The red shift of the optical band gap observed could be ascribed to the difference of structure type between the compounds.

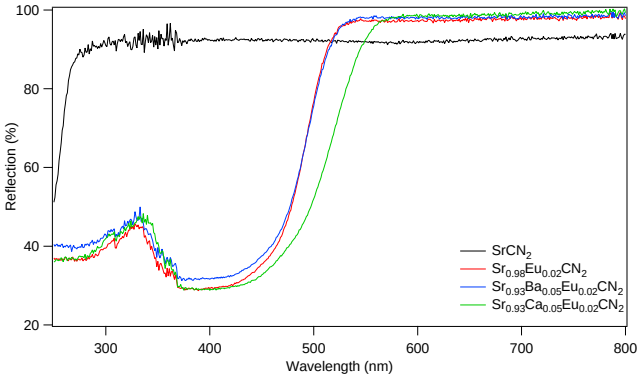

Figure 4: Reflection spectra of undoped ($SrCN_2$, black curve) and Eu^{2+} doped $SrCN_2$ samples ($Sr_{0.98}Eu_{0.02}CN_2$, $Sr_{0.93}Ba_{0.05}Eu_{0.02}CN_2$ and $Sr_{0.93}Ca_{0.05}Eu_{0.02}CN_2$, red, blue and green curves, respectively).

3.4. Photoluminescence properties at low temperatures

The luminescence spectra of Eu^{2+} doped $SrCN_2$ samples at 77 K are presented in Figure 5. By monitoring the emission at 620 nm, samples show an excitation spectrum in the wavelength region of 290-475 nm consisting of a broad band with several sub bands, which originate from the $4f^7 \rightarrow 4f^65d^1$ transitions of Eu^{2+}. Excited by 440 nm light, emission spectra of $Sr_{0.98}Eu_{0.02}CN_2$ shows a broad emission band centered at about 620 nm and full-width at half-maximum (FWHM) around 95 nm. For comparison, Yuan et al. and Krings et al. have reported a maximum emission at 610 nm (FWHM = 82 nm) and at 603 nm (FWHM = 137 nm) respectively [3, 4]. This broad emission band can be assigned to the allowed $4f^65d^1 \rightarrow 4f^7$ transition of Eu^{2+}. Moreover, there are no characteristic sharp peaks corresponding to Eu^{3+} luminescence which suggests that there is a full reduction from Eu^{3+} to Eu^{2+} in the synthesis process.

Table 2: Occupied Wyckoff sites, refined atomic coordinates (in Å), isotropic atomic displacement parameters B^{iso} (in Å^2) and site occupancies of $SrCN_2$, $Sr_{0.98}Eu_{0.02}CN_2$, $Sr_{0.93}Ba_{0.05}Eu_{0.02}CN_2$ and $Sr_{0.93}Ca_{0.05}Eu_{0.02}CN_2$ (standard deviation in parentheses).

Atom	Wyck.	x	y	z	B_{iso}	Occ.
			$SrCN_2$			
Sr	4c	0.1310(1)	1/4	0.1150(0)	0.91(4)	1
C	4c	0.378(2)	1/4	0.105(3)	0.7(4)	1
N1	4c	0.327 (1)	1/4	0.904(3)	1.3(3)	1
N2	4c	0.416(1)	1/4	0.305(2)	-0.05(4)	1
			$Sr_{0.98}Eu_{0.02}CN_2$			
Sr	4c	0.1310(2)	1/4	0.1136(4)	1.04(7)	0.98
Eu	4c	0.1310(2)	1/4	0.1136(4)	1.04(7)	0.02
C	4c	0.375(2)	1/4	0.091(3)	0.7(4)	1
N1	4c	0.329(1)	1/4	0.909(3)	0.4(3)	1
N2	4c	0.413(1)	1/4	0.306(3)	1.1(5)	1
			$Sr_{0.98}Eu_{0.02}CN_2$, $Sr_{0.93}Ba_{0.05}Eu_{0.02}CN_2$			
Sr	4c	0.1308(1)	1/4	0.1159(2)	1.15(5)	0.93
Ba	4c	0.1308(1)	1/4	0.1159(2)	1.15(5)	0.05
Eu	4c	0.1308(1)	1/4	0.1159(2)	1.15(5)	0.02
C	4c	0.378(1)	1/4	0.110(2)	0.9(3)	1
N1	4c	0.3258(6)	1/4	0.918(2)	0.5(2)	1
N2	4c	0.421(6)	1/4	0.317(2)	0.3(3)	1
			$Sr_{0.98}Eu_{0.02}CN_2$, $Sr_{0.93}Ca_{0.05}Eu_{0.02}CN_2$			
Sr	3b	1/3	2/3	1/6	1.06(7)	0.93
Ca	3b	1/3	2/3	1/6	1.06(7)	0.05
Eu	3b	1/3	2/3	1/6	1.06(7)	0.02
C	3a	0	0	0	0.6(3)	1
N	6c	0	0	0.8205(4)	0.8(2)	1

For $Sr_{0.93}Ba_{0.05}Eu_{0.02}CN_2$, the emission band shifts to longer wavelength and is centered at about 630 nm with a much wider full-width at half-maximum around 165 nm. The very small red shift (~ 10 nm) of the emission band can be attributed to the structural change after substitution by Ba^{2+} leading to the reduction of bond length disparity. Compared with the average Sr–N bond length of $Sr_{0.98}Eu_{0.02}CN_2$ (i.e. 2.651 Å), the value decreases after substitution by Ba^{2+} (i.e. 2.638 Å) which give rises to a stronger crystal field splitting of 5d states of Eu^{2+} and consequently to the experimentally observed red shift. While almost no disparity is observed in the Sr–N bond lengths based on the Rietveld refinement of the average lattice for the Ba^{2+} substituted $SrCN_2$, the much larger size of Ba^{2+} vs. Sr^{2+} is likely to induce local distortions resulting in a variety of coordination environment for the Eu^{2+} luminescent center, thus leading to the broadening of the emission. In contrast, the emission spectra profile of $Sr_{0.93}Ca_{0.05}Eu_{0.02}CN_2$ which presents the β-type structure is similar to that of $Sr_{0.98}Eu_{0.02}CN_2$. However, the intensity of the emission band of Ca^{2+} substituted sample was significantly higher than that of $Sr_{0.98}Eu_{0.02}CN_2$ and $Sr_{0.93}Ba_{0.05}Eu_{0.02}CN_2$. This huge difference in emission intensity forced us to reduce the monochromators slit widths of the fluorimeter in order to avoid detector saturation. In that respect, only normalized emission spectra of samples are displayed. The effect of temperature on emission was investigated between 77 and 197 K using excitation wavelength of 440 nm. As shown in Figure 6 and Figures S5 to S7, the emission of Eu^{2+} doped $SrCN_2$ samples is strongly quenched with increasing temperatures. The temperatures at which the emission intensity is reduced by 50% (T1/2) were approximately 82 K for $Sr_{0.98}Eu_{0.02}CN_2$ and 87 K for $Sr_{0.93}Ba_{0.05}Eu_{0.02}CN_2$ and $Sr_{0.93}Ca_{0.05}Eu_{0.02}CN_2$. At 197 K the emission intensities of samples are totally quenched. These results confirm those already published by Yuan et al. [3] indicating a total quenching of the emission at 227 K for Eu^{2+} doped α-$SrCN_2$ and are in total contrast to the results reported by Krings et al. [4] which describe a room temperature orange emission.

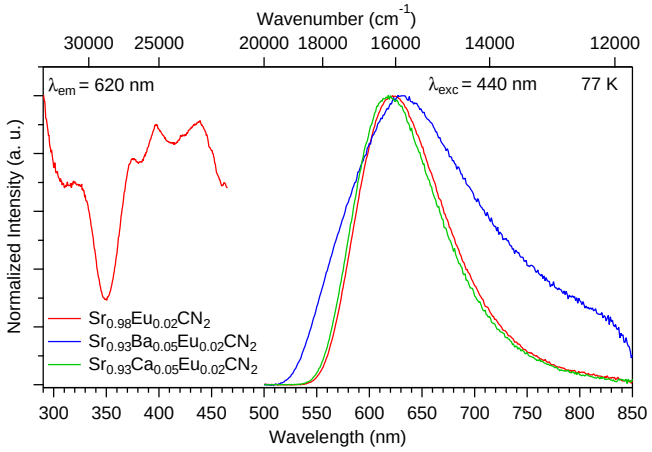

Figure 5: Normalized excitation (λ_{em} = 620nm) and emission (λ_{ex} = 440 nm) spectra of $Sr_{0.98}Eu_{0.02}CN_2$ (red curves), $Sr_{0.93}Ba_{0.05}Eu_{0.02}CN_2$ (blue curve) and $Sr_{0.93}Ca_{0.05}Eu_{0.02}CN_2$ (green curve) at 77 K.

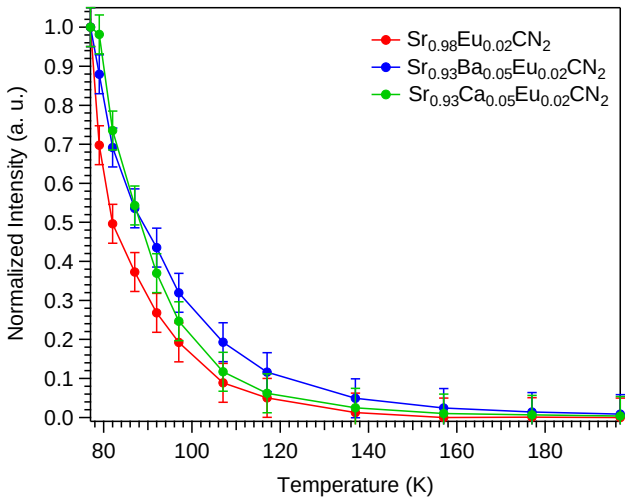

Figure 6: Normalized emission intensity (integrated area) vs temperature (77 - 197 K) for $Sr_{0.98}Eu_{0.02}CN_2$ (red dots), $Sr_{0.93}Ba_{0.05}Eu_{0.02}CN_2$ (blue dots), $Sr_{0.93}Ca_{0.05}Eu_{0.02}CN_2$ (green dots). Uncertainty bar = ±0.05.

4. Conclusion

In this paper, we have reported a new simple and efficient synthetic route allowing the obtaining of highly crystallized strontium carbodiimide ($SrCN_2$) materials in just one hour under NH_3 atmosphere at moderate temperature. Single phase Eu^{2+} doped α- and β-polymorphs were obtained in a reproductible manner using the same experimental conditions through the substitution of Sr^{2+} by a larger (Ba^{2+}) or smaller cation (Ca^{2+}), respectively. The impact of the crystalline structure on the photoluminescence properties of Eu^{2+} doped $SrCN_2$ has been investigated. Both single phases showed orange emission with peaks at 620 nm for $Sr_{0.98}Eu_{0.02}CN_2$ and $Sr_{0.93}Ca_{0.05}Eu_{0.02}CN_2$ and 630 nm for $Sr_{0.93}Ba_{0.05}Eu_{0.02}CN_2$ at 77 K under 440 nm light excitation. Thermal quenching of luminescent properties was observed with increasing temperature for both α- and β-structure. Temperatures at which the emission intensity is reduced by 50% is comprised between 82 K and 87 K, and at 197 K the emission is completely quenched.

References

[1] P. Pust, P. Schmidt, W. Schnick, A revolution in lighting, Nat. Mater. 14 (2015) 454–458. doi:10.1038/nmat4270.

[2] S. Pimputkar, J. Speck, S. DenBaars, S. Nakamura, Prospects for led lighting, Nat. Photon. 3 (2009) 180–182. doi:10.1038/nphoton.2009.32.

[3] S. Yuan, Y. Yang, F. Cheviré, F. Tessier, X. Zhang, G. Chen, Photoluminescence of Eu^{2+}-doped strontium cyanamide: A novel host lattice for Eu^{2+}, J. Amer. Ceram. Soc. 93 (2010) 3052–3055. doi:10.1111/j.1551-2916.2010.04025.x.

[4] M. Krings, G. Montana, R. Dronskowski, C. Wickleder, α-SrNCN:Eu^{2+} - a novel efficient orange-emitting phosphor, Chem. Mater. 23 (2011) 1694–1699. doi:10.1021/cm102262u.

[5] Y. Masubuchi, S. Nishitani, A. Hosono, Y. Kitagawa, J. Ueda, S. Tanabe, H. Yamane, M. Higuchi, S. Kikkawa, Red-emission over a wide range of wavelengths at various temperatures from tetragonal $BaCN_2$:Eu^{2+}, J. Mater. Chem. C 6 (2018) 6370–6377. doi:10.1039/C8TC01289J.

[6] M. Kubus, C. Castro, D. Enseling, T. Jüstel, Room temperature red emitting carbodiimide compound $Ca(CN_2)$:Mn^{2+}, Opt. Mater. 59 (2016) 126–129. doi:10.1016/j.optmat.2016.01.006.

[7] U. Berger, W. Schnick, Syntheses, crystal structures, and vibrational spectroscopic properties of $MgCN_2$, $SrCN_2$, and $BaCN_2$, J. Alloys Compd. 206 (1994) 179–184. doi:10.1016/0925-8388(94)90032-9.

[8] W. Liao, R. Dronskowski, β-strontium carbodiimide, Acta Cryst. E 60 (2004) i124–i126. doi:10.1107/S1600536804023244.

[9] J. Liu, J. Sun, C. Shi, A new luminescent material: Li_2CaSiO_4:Eu^{2+}, Mater. Lett. 60 (2006) 2830–2833. doi:10.1016/j.matlet.2006.01.100.

[10] J. Rodríguez-Carvajal, Recent advances in magnetic structure determination by neutron powder diffraction, Physica B: Condensed Matter. 192 (1993) 55–69. doi:10.1016/0921-4526(93)90108-I.

[11] T. Roisnel, J. Rodriguez-Carvajal, Winplotr: A windows tool for powder diffraction pattern analysis, Mater. Sci. Forum: European Powder Diffraction EPDIC7 378-381 (2001) 118–123. doi:10.4028/www.scientific.net/MSF.378-381.118.

[12] J.-F. Bérar, P. Lelann, E.s.d.'s and estimated probable error obtained in rietveld refinements with local correlations, J. Appl. Cryst. 24 (1991) 1–5. doi:10.1107/S0021889890008391.

[13] J.-F. Bérar, Data optimization and propagation of errors in powder diffraction, "Acc. Pow. Diff II", NIST sp. Pub 846 (1992) 63.

[14] D. Kubelka, L. Munk, Ein beitrag zur optik der farbanstriche, Z. Tech. Phys. 12 (1931) 593–601.

[15] A. Perret, A. Krawezynski, Recherches sur les cyanamides métalliques, Helv. Chim. Acta 15 (1992) 1009–1022. doi:10.1002/hlca.193201501111.

[16] M. Krings, M. Wessel, W. Wilsmann, P. Müller, R. Dronskowski, Temperature-dependent synthetic routes to and thermochemical ranking of α- and β-SrNCN, Inorg. Chem. 49 (2010) 2267–2272. doi:10.1021/ic902065q.

[17] A. Thomas, A. Fischer, F. Goettmann, M. Antonietti, J.-O. Müller, R. Schlögl, J. M. Carlsson, Graphitic carbon nitride materials: variation of structure and morphology and their use as metal-free catalysts, J. Mater. Chem. 18 (2008) 4893–4908. doi:10.1039/B800274F.

[18] T. Takeda, N. Hatta, S. Kikkawa, Ammonia nitridation synthesis and structural change of strontium cyanamide polymorphs, J. Ceram. Soc. Jpn. 115 (2007) 729–731. doi:10.2109/jcersj2.115.729.

5. Supporting Information

Table S1: EDS analyses of $SrCN_2$ compounds.

	Sr (at%)	Eu (at%)	Ba (at%)	Ca (at%)	Na (at%)
$SrCN_2$	100	-	-	-	0
$Sr_{0.98}Eu_{0.02}CN_2$	97.53	2.47	-	-	0
$Sr_{0.93}Ba_{0.05}Eu_{0.02}CN_2$	91.24	2.88	5.88	-	0
$Sr_{0.93}Ca_{0.05}Eu_{0.02}CN_2$	92.44	2.41	-	5.15	0

Table S2: Selected bond distances of $SrCN_2$ compounds.

Bonds	Distances (Å)
	$SrCN_2$
Sr–N	2.5754 (x2), 2.6585 (x2), 2.6882, 2.7060
C–N	1.1778, 1.2559
	$Sr_{0.98}Eu_{0.02}CN_2$
Sr–N	2.5833 (x2), 2.6437 (x2), 2.7096, 2.7449
C–N	1.1340, 1.2549
	$Sr_{0.93}Ba_{0.05}Eu_{0.02}CN_2$
Sr–N	2.6261(x2), 2.6429 (x2), 2.6347, 2.6585
C–N	1.2295, 1.2339
	$Sr_{0.93}Ca_{0.05}Eu_{0.02}CN_2$
Sr–N	2.6150 (x6)
C–N	1.1778

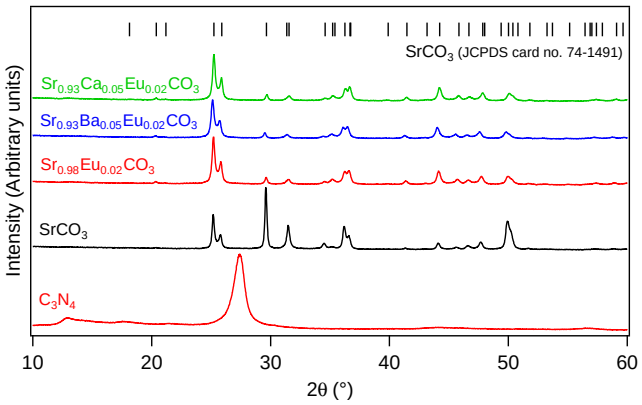

Figure S1: Powder XRD patterns of the as prepared carbon nitride and carbonates precursors.

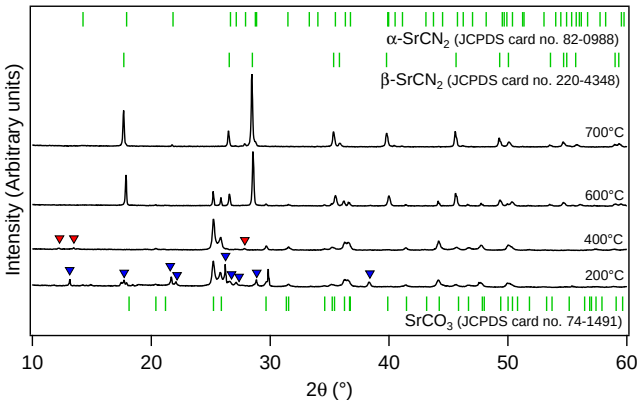

Figure S2: Powder XRD patterns of the products obtained from mixtures of H_2CN_2 and $SrCO_3$ at various temperatures. Blue triangles indicate extra-peaks corresponding to melamine phase while red triangles indicate extra-peaks corresponding to melem phase.

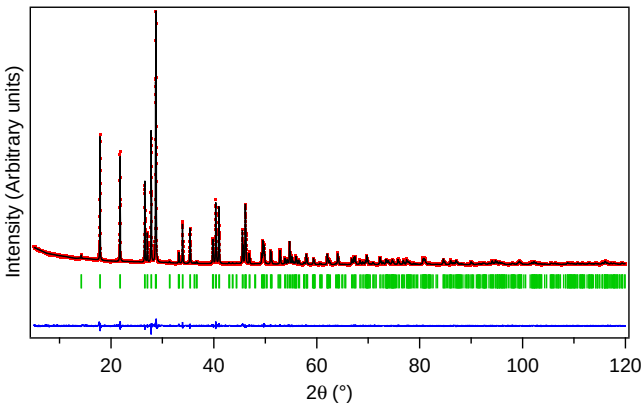

Figure S3: Final Rietveld refinement pattern for $Sr_{0.93}Ba_{0.05}Eu_{0.02}CN_2$: observed (red dotted line), calculated (black full line) and difference (blue line) X-ray powder diffraction profiles from the pattern matching plot obtained with Fullprof. The vertical markers correspond to the position of the Bragg reflections.

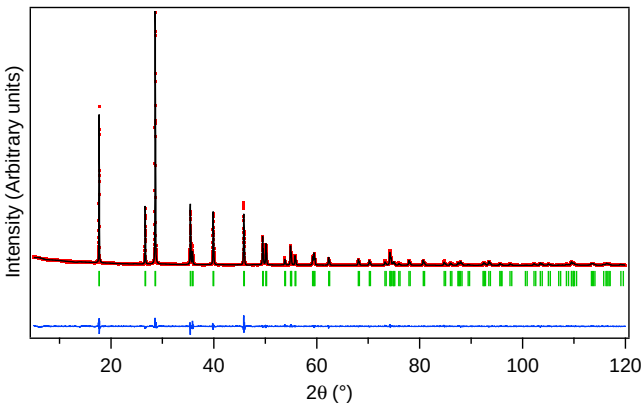

Figure S4: Final Rietveld refinement pattern for $Sr_{0.93}Ca_{0.05}Eu_{0.02}CN_2$: observed (red dotted line), calculated (black full line) and difference (blue line) X-ray powder diffraction profiles from the pattern matching plot obtained with Fullprof. The vertical markers correspond to the position of the Bragg reflections.

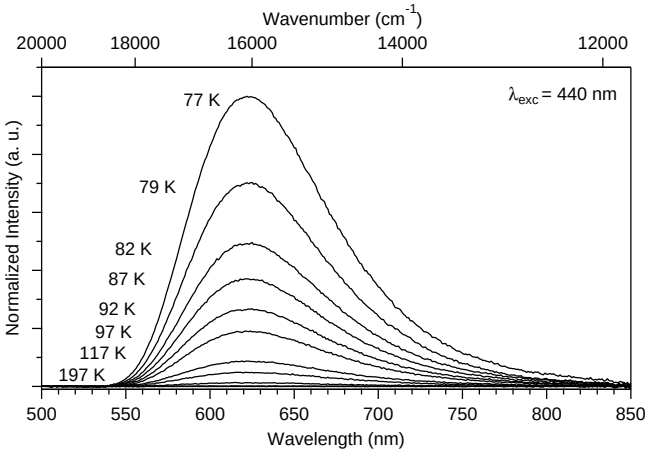

Figure S5: Emission (λ_{ex} = 440 nm) spectra of $Sr_{0.98}0.05Eu_{0.02}CN_2$ at variable temperature (77 - 197 K).

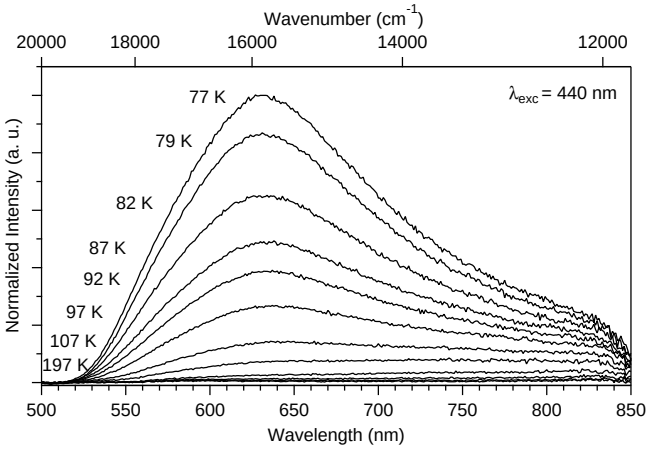

Figure S6: Emission (λ_{ex} = 440 nm) spectra of $Sr_{0.93}Ba_{0.05}Eu_{0.02}CN_2$ at variable temperature (77 - 197 K).

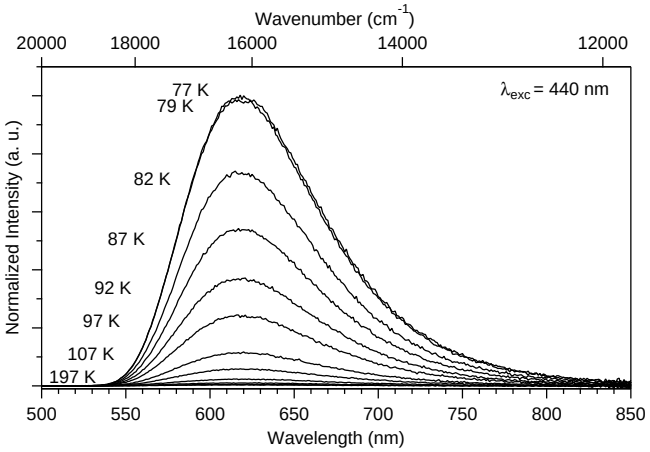

Figure S7: Emission (λ_{ex} = 440 nm) spectra of $Sr_{0.93}Ca_{0.05}Eu_{0.02}CN_2$ at variable temperature (77 - 197 K).